

Implementing Reinforcement Learning Datacenter Congestion Control in NVIDIA NICs

Benjamin Fuhrer¹ Yuval Shpigelman¹ Chen Tessler² Shie Mannor^{2,3} Gal Chechik^{2,4} Eitan Zahavi¹ Gal Dalal²

¹ NVIDIA Networking, ² NVIDIA Research, ³ Technion Institute of Technology, ⁴ Bar-Ilan University
{bfuhrer,yuvals,ctessler,smannor,gchechik,eitan,gdalal}@nvidia.com

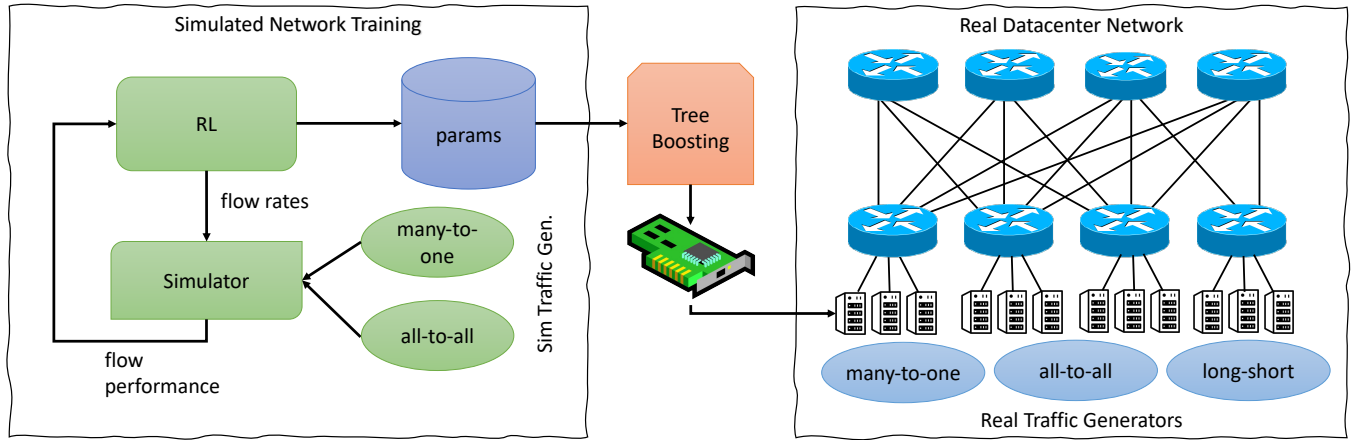


Figure 1: The entire flow: from reinforcement learning in simulation to live datacenter congestion control.

ABSTRACT

Cloud datacenters are exponentially growing both in numbers and size. This increase results in a network activity surge that warrants better congestion avoidance. The resulting challenge is two-fold: (i) designing algorithms that can be custom-tuned to the complex traffic patterns of a given data-center; but, at the same time (ii) run on low-level hardware with the required low latency of effective Congestion Control (CC). In this work, we present a Reinforcement Learning (RL) based CC solution that learns from certain traffic scenarios and successfully generalizes to others. We then distill the RL neural network policy into binary decision trees to achieve the desired μsec decision latency required for real-time inference with RDMA. We deploy the distilled policy on NVIDIA NICs in a real network and demonstrate state-of-the-art performance, balancing all tested metrics simultaneously: bandwidth, latency, fairness, and packet drops.

CCS CONCEPTS

• **Computing methodologies** → **Reinforcement learning**; **Neural networks**; **Classification and regression trees**;
• **Networks** → **Transport protocols**; • **Datacenter Networks**;

KEYWORDS

RDMA, Datacenter Networks, Congestion Control, Reinforcement Learning, Neural Networks, , Distillation, Boosting Trees

1 INTRODUCTION

Modern datacenters support computationally intensive applications such as distributed data processing, heterogeneous and edge computing, and storage. With advancements in hardware and software, networks can support bandwidths of up to 400Gbps (e.g., Nvidia ConnectX-7 [9]). At such speeds, the typical remote memory access, traditionally handled by the remote CPU, becomes a bottleneck. CPU over-utilization also leads to application delays and an increase in operational costs. A natural solution is to offload memory management to the network interface card (NIC). Remote Direct Memory Access (RDMA) and RDMA over converged Ethernet (RoCEv2) [4] provide protocols that bypass the CPU, resulting in lower CPU overhead. Consequently, RDMA has been increasingly adopted in datacenter networks [18].

With the latency reduction achieved by increased rates and RDMA, the limiting factor in network performance becomes traffic congestion. Congestion occurs when traffic arrives

at a node (switch or NIC) at a faster rate than it can be processed. As each node is equipped with a first-in-first-out (FIFO) queue, the transmission latency grows proportionally to the congestion. Efficient CC is thus crucial to sustaining high throughput and low latency in datacenters. CC algorithms set a limit on the transmission rate or number of in-network bytes of each flow. By observing changes in the network, such as latency and telemetry signals, these algorithms are tasked with preventing congestion in a diverse set of network topologies and traffic patterns.

Most literature on CC tackled the problem using hand-crafted heuristics. These methods tend to perform exceptionally well in a specific set of tasks yet under-perform in others that they were not optimized for. For instance, DCQCN [53] and SWIFT [25] have been optimized for steady-state scenarios; but, as shown in [44], their reaction time is slow for sudden bursts of short flows. Recently, Tessler et al. [44] introduced a data-driven approach to learning a CC policy. They presented a reward function (measuring the latency and throughput) and devised an algorithm that maximizes the cumulative reward throughout multiple steps. Their method resulted in a robust policy capable of tackling a range of tasks in a *simulated* network. Despite its impressive results, their method has two major flaws that hinder its applicability – reliance on round-trip-latency (RTT) measurements and long inference time. The former is less indicative compared to the more accurate telemetry information such as queue-length [29], while the latter prevents leveraging the advantages of RDMA.

In this work, we overcome the above issues that prevented ML-based CC approaches from reaching production pipelines. We design an RL algorithm that achieves state-of-the-art (SOTA) performance and, at a second phase, reshape it to comply to present hardware limitation. We also analyze our algorithm’s behavior in a human-interpretable fashion and show how it matches known concepts in classic CC theory. In summary, our main contributions are:

- (1) We show how to map complex policies to low-compute low-latency architecture, gaining x500 latency reduction with a negligible effect on the quality of the policy. Specifically, we map deep networks with 450 μsec latency to decision trees with 0.9 μsec latency.
- (2) We improve the optimization objective presented in [44], cast RTT dependence to switch queue utilization, and analyze the controllable reward parameters.
- (3) We deploy our method on NVIDIA production NICs, ConnectX-6Dx, in an operational cluster of 64 hosts, and run extensive evaluations reaching SOTA results.

The RL-CC framework is visualized in Fig. 1.

2 BACKGROUND AND PROBLEM SETUP

In this section we provide an overview of relevant background and prior work, and formulate the problem setup.

2.1 Congestion Control

RoCEv2 can be implemented in both lossless and lossy networks [42]. In lossless networks, the Priority Flow Control (PFC) prevents packet drops by pausing transmission. This behavior has been shown to result in poor flow performance and cause other problems such as deadlock [20, 53]. On the other hand, in lossy networks, dropped packets are re-transmitted, resulting in a reduction of goodput bandwidth and increased latency. CC algorithms have been demonstrated to minimize PFC activation in lossless networks and reduce packet drops in lossy networks, thus improving overall network performance [7, 25, 33, 42, 49, 51–53]. These methods govern the transmission rate of each flow, while balancing multiple, possibly conflicting, objectives. They aim to maximize the overall network utilization and fairness between flows, while minimizing packet latency and packet drops, all while reacting rapidly to changes.

The conflict between these objectives was explained by Kumar et al. [25]: when N flows share a congested path, and each transmits at the optimal rate (line rate/ N), the average queue length is $O(\sqrt{N})$. Hence, a low latency solution that is fair when N is large can only be achieved by reducing bandwidth, resulting in a bandwidth-latency tradeoff. While the above tradeoff is clear when in steady state, CC algorithms must also adapt rapidly to changes and converge to a new equilibrium. This can happen when flows abruptly stop transmitting, or alternatively when new ones join and start transmitting. Maintaining a stable steady state and reacting quickly to changes are two contradictory abilities. High sensitivity to changes in transmission rate impair convergence to a stable point. Contrarily, small changes to the transmission rate may cause it to converge too slowly, resulting in packet drops or under-utilization.

2.2 Existing State-of-the-Art for CC

Current SOTA CC relies on indications such as end-to-end delay and switch queue-length to evaluate the network’s status and adjust the transmission rate appropriately. Those deployed in practice use rule-based heuristics to react to such indications. For instance, DCQCN [53], a popular CC algorithm in datacenter deployments, utilizes Explicit Congestion Notification (ECN) [17]. As ECN packets are statistical indications of a developing congestion, DCQCN cuts down the transmission rate once such packets are observed. Other algorithms like Timely [33] and Swift [25] rely on end-to-end delay for making decisions. Lastly, HPCC [29] takes as

input the switch queue length and port bandwidth. This information, called telemetry, is only accessible in datacenter networks with appropriate hardware support.

Varying traffic patterns and network topologies result in different indicator statistics. Thus, a common drawback of conventional CC algorithms is the need for manual tuning of their multiple parameters. Such tuning necessitates laborious calibrations by domain experts. And yet, the results are often unsatisfactory at properly balancing the tradeoffs (Section 2.1). For example, DCQCN excels at stability in steady-state workloads such as storage but is slow to adapt to more dynamic compute-heavy workloads [29]. HPCC, on the other hand, is a top-performer in dynamic workloads at the expense of stability and high utilization during steady-state scenarios [7].

2.3 Transmission Rate Modulation

CC is typically conducted by setting a maximum transmission rate per flow (rate-limiting). Traditionally, transmission rate modulation uses additive increases and multiplicative decreases (AIMD) [13]. Chiu and Jain [13] showed that by performing a fixed additive increase while congestion is not observed and halving the transmission rate otherwise, AIMD converges to a fair solution where all flows utilize an equal share of the bottleneck. In addition, they showed that other additive/multiplicative variations, AIAD, MIAD, and MIMD, do not reach fair solutions.

With the emergence of high-speed links, the classic AIMD algorithm proved to under-utilize link capacity [16]. Since then, CC algorithms have evolved, and more sophisticated methods to modulate transmission rates have been proposed. For instance, DCQCN uses AIMD yet adjusts both the additive increase magnitude and the multiplicative decrease. It increases rate by multiple successive increases towards a target rate, followed slow increments of the target rate itself. Once congestion is observed, it shrinks the transmission rate by α , a parameter that is dynamically adjusted by the algorithm. Similarly, Swift is also an AIMD variant. When receiving an ACK packet, Swift uses the difference between a flow’s delay and a target value to determine the rate change. In contrast, HPCC applies both AIMD and MIMD to avoid congestion. AIMD is used to sustain a stable steady-state, while MIMD is used when changes in the network occur and rapid reaction is necessary to reclaim bandwidth.

Due to its excellent stability property, the prior works described above and others mostly focused on AIMD. MIMD, on the other hand, is trickier; while it allows faster recovery and lower packet latency, it requires carefully tuning to be able to reliably reach convergence. This is where artificial intelligence (AI) naturally fits in to fulfill its promise of adaptively tuning its behavior within complex data patterns.

2.4 AI-based CC

Machine learning (ML) was successfully implemented across disciplines, ranging from healthcare to autonomous driving. Compared to manual tuning methods, ML algorithms are capable of extracting complex patterns from vast amounts of data, learning implicit correlations that enable better generalization and performance [22]. Prior work considered ML-based CC; however, those algorithms often require large memory and computational complexity [22]. Generally, for CC algorithms to successfully operate, their decision time must be $O(\text{RTT})$. For modern datacenters utilizing RDMA, this amounts to a few μsec . These limitations partly explain why there is currently no learning-based CC in production.

Recently, Tessler et al. [44] introduced an RL-based RDMA CC algorithm called Analytic Deterministic Policy Gradient (ADPG). In several network simulation benchmarks, ADPG outperformed SOTA rule-based CC algorithms: DCQCN, SWIFT, and HPCC. Its success is partially attributed to MIMD, where the increase/decrease values are a function of the historically observed congestion. Another crucial component in the success of ADPG is its RTT-based reward that at its optimum depicts an optimal flow equilibrium. In line with our summary above, Tessler et al. [44] state that for potential deployment, they would require dedicated hardware to accommodate the computational burden of deep-learning inference. In this work, we build upon [44] and devise a reward-modified variant which we call RL-CC. As we show later, we also solve the computational challenge flagged by Tessler et al. [44].

2.5 Problem Setup

We consider two environment settings – simulation and live. For simulation, we utilize a realistic OMNeT++ emulator [45] that models a shallow single-switch network with a varying number of flows. We experiment with different combinations of total flows, ranging between 2 – 8192, distributed across multiple hosts. Each host is equipped with an NVIDIA NIC. With the simulator, we train the RL agent on a small set of benchmarks and then evaluate them on larger ones, with precise in-network measurements at pinpoint accuracy. While the simulations are rich, they do not precisely mimic real-world behavior. For instance, they do not emulate complex network topologies and their effect on congestion and RTT. Thus, we also perform experiments on two operational clusters detailed in Section 6.1. Next, we list the experiments we perform.

Many to one: All hosts transmit data to a single receiver host. This tests the ability of multiple flows, sharing a single congestion path, to converge to a stable fair solution. The ideal solution is when all N flows transmit at $\frac{\text{line rate}}{N}$.

All to all: All hosts transmits data to all others. This tests the algorithm’s ability to operate under high stress and uncertainty.

Long Short: A single long flow transmits unlimited data, while multiple short flows randomly appear and transmit for a short window of time. As opposed to many-to-one and all-to-all, which are steady-state tests, Long-Short is a transient test. In this test, we evaluate the rapidness in which the long flow reacts – once, when the short flows begin transmitting, and the second time when they seize.

We evaluate our experiments with different metrics for the steady-state experiments and for the recovery experiments.

Steady-state - (i) goodput bandwidth, (ii) unfairness calculated as the coefficient of variation of the sent bandwidth per host, (iii) average packet latency, and (iv) average packet loss per flow. Higher \uparrow is better for metric (i), while lower \downarrow is better for (ii, iii, iv).

Recovery - (i) long flow bandwidth, (ii) average packet loss per flow (iii) average normalized completion time, (iv) normalized completion time 99% percentile. Bigger is better for metric (i), while lower is better for (ii, iii, iv).

In this work, we compare the performance of RL-CC to the Swift heuristic [25], as it also relies on the **target** parameter. Additionally, we compare our final implementation to the hardware built-in DCQCN.

3 RL FOR CC

Congestion control is a sequential decision-making problem. The decision maker in our case is an instance of the CC algorithm running within the NIC and controlling the rate of a single transmission flow. From here on, we refer to it as an *agent*. The agent acts upon recent information available to it: current and past transmission rate, RTT, and last actions taken. The agent’s biggest challenge is that it is completely unaware of the existence of other concurrent agents and their state. It needs to act strictly based on its local state where all global network sensing is based solely on RTT packets the agent receives.

Formally, this task is modeled as a multi-agent partially-observable Markov decision process (POMDP) [44], defined as the tuple $(O, S, \mathcal{A}, P, R)$ [38]. The agent is always at some state $s \in S$ and observes the corresponding observation $o(s) \in O$. Based on o , the agent selects a continuous action $a \in \mathcal{A}$. In a POMDP, in contrast to a fully-observable MDP, the observation does not necessarily contain sufficient statistics to determine the optimal action. After performing an action, the environment transitions to a new state s' based on the probabilistic transition kernel $P(s' | s, a)$, and the agent is receives reward $r(s, a) \in R$ and a new observation $o(s')$.

A policy $\pi : O \rightarrow \mathcal{A}$ is a mapping from observations to actions. Our goal is to find an optimal policy which maximizes

$\rho^\pi(s)$: the *average reward* along the expected trajectory w.r.t. P when starting from state s . We denote the optimal policy by π^* , yielding the optimal gain ρ^* , i.e., one that maximizes the average reward from any initial state.

Modern NVIDIA NICs support programmable CC engines and network state measurements such as RTT or switch telemetry. Leveraging this mechanism, we implement an RL agent that observes relevant statistics performs MIMD transmission rate modulation actions. More explicitly, the environment consists of:

Observations. The agent observes information relevant only to the flow it controls: present and past transmission rate and RTT measurement. When telemetry is available, we replace the RTT measurement with the switch queue length.

Actions. At time t , the agent decides on an action a_t that modifies the next transmission rate in a multiplicative manner such that $\text{rate}_{t+1} = a_t \cdot \text{rate}_t$.

Transitions. The transition $s_t \rightarrow s_{t+1}$ depends on the dynamics of the environment and occurs when the agent is polled to provide an action. We follow prior work and consider event-triggered decision-making, where the agent acts immediately after receiving an RTT measurement.

Reward. Kumar et al. [25] have shown that when N flows share a congested path and transmit at the ideal rate of $\frac{\text{max rate}}{N}$ then the average queue length is $O(\sqrt{N})$. Denoting the i -th flow’s RTT inflation at time t by $\text{RTT-inflation}_t^i = \frac{\text{RTT}_t^i}{\text{base-RTT}^i}$, we extend the reward from [44] and define the reward obtained by agent i controlling flow i at time t as:

$$r_t^i = - \left(\text{target} - \max(\text{RTT-inflation}_t^i - \beta, 0) \cdot \sqrt{\text{rate}_t^i} \right)^2, \quad (1)$$

where **target** is the inflation control parameter, β is the congestion tolerance, and base-RTT^i is the i -th flow’s RTT measurement in an empty system. In the following sections we provide an extensive analysis of how the user-chosen parameters **target** and β affect the agent’s behavior.

The main benefit of this reward design is that the system achieves a fixed-point equilibrium when the reward is maximal, i.e. $r = 0$. Substituting $O(\sqrt{N})$ for the rate, it can be easily seen that the rate $= O(\frac{1}{\sqrt{N}})$, and when $\text{RTT-inflation} > \beta$, the expected RTT-inflation at steady-state is expressed as:

$$\mathbb{E}[\text{RTT-inflation}] = \text{target} \cdot \sqrt{N} + \beta. \quad (2)$$

Policy optimization: The CC environment is particularly challenging compared to the standard MDPs that RL algorithms usually tackle. Namely, it constitutes a unique combination of a partially-observable multi-agent system with multiple objectives and that is also non-stationary. For these reasons, Tessler et al. [44] developed the custom-made ADPG method – a deterministic on-policy algorithm that leverages the access to the analytical form of the reward

function. Here, we build upon [44] and introduce a modified variant of ADPG which we refer to as RL-CC. For RL-CC, we obtain the policy gradient approximation

$$\nabla_{\theta} \rho^{\pi_{\theta}}(s^i) \approx \left[\lim_{T \rightarrow \infty} \frac{1}{T} \sum_{t=0}^T \left(\text{target} - \max(\text{RTT-inflation}_t^i - \beta, 0) \cdot \sqrt{\text{rate}_t^i} \right) \nabla_{\theta} \pi_{\theta}(o(s^i)) \right] \quad (3)$$

For ease of notation, we define:

$$\delta_t^i = \text{target} - \max(\text{RTT-inflation}_t^i - \beta, 0) \cdot \sqrt{\text{rate}_t^i} \quad (4)$$

For states in which $\delta_t^i < 0$, a negative weight is assigned to the gradient of the policy, effectively reducing the transmission rate at those states, and vice-versa for $\delta_t^i > 0$. Furthermore, $\delta_t^i \in [-\infty, \text{target}]$ is bounded from above as the minimal RTT inflation is 0, but not from below as the latency can grow arbitrarily large. As a result the policy is influenced to react more aggressively towards congestion.

RL-CC’s architecture [44] was originally composed of two fully-connected layers (input $\rightarrow 32 \rightarrow 16$) followed by an LSTM layer [19] ($16 \rightarrow 16$) and then an output fully-connected layer ($16 \rightarrow 1$). The input is the current state, s_t , a tuple (δ_t, a_{t-1}) , the current observation and the previously taken action. The LSTM allows the policy to incorporate past information into the decision, enabling it to handle the partial observability of the environment. In Section 4 we follow the LSTM architecture described above. In Section 4.1 we utilize a lighter MLP-based architecture that can be simply analyzed and explained. This same MLP architecture is later used in Section 5.1, where it is then distilled into a tree-based policy that can be implemented in an NVIDIA NIC.

4 ANALYSIS OF RL-CC

In this section, we study the behavior of RL-CC from various angles. We begin with a comparison of theory versus practice and show how well the performance observed in simulation matches the theoretical expected performance. Afterwards, we explain the role of the controllable parameters **target** and β , and analyze their effect on RL-CC’s behavior. We performed all simulation in this section with OMNeT++ in a single switch, 4 hosts to 1 (Many-to-One) scenario, for 1 simulated sec. Unless mentioned otherwise, we repeated the experiment with different numbers of flows per host and collected the data for a period of 0.5 sec after reaching a steady-state. For our parameters, we used **target** = 0.064, β = 1.5.

Theory versus practice: In Fig. 2, we compare the RTT inflation in theory, either as given in Eq. (2), or as an appropriately fitted $O(\sqrt{N})$ curve to that obtained by our trained policy and Swift’s respectively, in simulation. As

seen, the RL-CC and the theoretical curve are almost identical for a wide range of participating flows. This verifies that by optimizing the reward, the agent converges to an optimal policy that maintains a saturated link with steady RTT where all flows transmit at a similar rate. However, as the number of flows grows, Swift diverges from the fitted curve. We attribute this fact to Swift’s AIMD procedure. As the rate adjustment is higher (in percentage) when the rate is low, the additive increase becomes more aggressive when the number of flows is large. This results in overshoots, impacting the latency unfavorably.

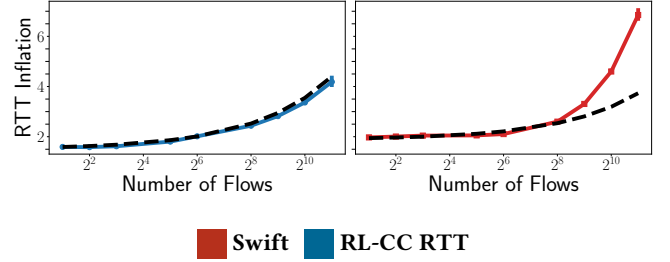


Figure 2: RL-CC and Swift Theory vs. Practice: RTT inflation as a function of number of flows. Curved lines represent the theoretical curves in the order of $O(\sqrt{N})$. We plot the average RTT inflation per flow with 99% vertical confidence intervals. Error bars are small initially and grow as the number of flows increase.

Reward design: RTT may increase even when the combined transmission rate of all flows is below the maximal rate. This increase is due to stochastic collisions between flows [25] and results in a premature reaction. The congestion tolerance parameter, β , prevents this behavior by encouraging flows to increase their transmission rate as long as the RTT delay is below a pre-determined threshold. As a result, the bandwidth is increased when the number of flows is small. Moreover, β ’s significance diminishes when the number of flows increases, resulting in a minor impact on the delay when the number of flows is large. Once the RTT inflation surpasses β , the algorithm becomes sensitive to inflation indications. At this stage, the **target** controls the bandwidth-latency tradeoff.

Kumar et al. [25] have demonstrated that increasing the **target** value increases bandwidth at the expense of latency. Therefore, we aim to choose the lowest possible **target** to reduce latency while preserving a competitive bandwidth. Furthermore, they showed that the bandwidth drops rapidly below a certain **target** value. The exact **target** lower bound is a function of the network’s characteristics. In Fig. 3 we present an ablation study of several values, both for **target** and β . We observe that due to the reward function’s behavior and the system’s statistical nature, a low β results in

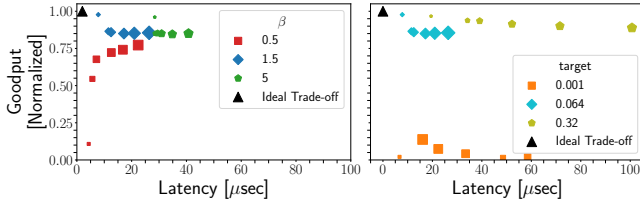


Figure 3: RL-CC parameter influence on the bandwidth/latency tradeoff. Left) Varying β . Right) Varying target. Marker size are proportional to the number of flows in the scenario.

instability when the number of flows is small. The plot also demonstrates how a higher **target** results in higher throughput, yet also higher latency. On the other hand, when the **target** is too small, the system is required to maintain a near-empty queue, which results in unstable performance.

From RTT to queue length: Up to here, we used RTT as the feedback for the agent. Indeed, it is a popular and widely available signal in most existing hardware, and is agnostic to the switches in the network. However, the base-RTT varies between hosts according to their physical position in the datacenter. Hence, when specialized switches are present, it is of interest to utilize them for more robust congestion indicators.

We now assume that the system is not under-utilized and that the maximum rate is identical between all switches in the network. It is well known that the i -th flow's RTT can be expressed as a linear function of the sum of queue lengths over all switches:

$$RTT^i[time] = \text{base-RTT}^i[time] + \frac{\sum_{k=1}^K \text{Queue Length}_k[\text{bytes}]}{\text{max rate}[\frac{\text{bytes}}{\text{time}}]} \quad (5)$$

By re-arranging the equation we have

$$\text{RTT-inflation}^i = 1 + \frac{\sum_{k=1}^K \text{Queue Length}_k}{\text{base-RTT}^i \cdot \text{max rate}} \quad (6)$$

We follow the approach introduced by Li et al. [29] and look at the most congested port along a flow's path as an indication.

Comparing to SOTA CC: In Fig. 4, we show how the RL-CC compares to Swift, with both the RTT and Queue Length versions. For both, RL-CC maintains better bandwidth to latency tradeoff. Swift sustains a higher goodput and similar latency to RL-CC when the number of flows is low. However, RL-CC demonstrates favorable goodput and latency when the number of increases, affirming the results shown in Fig. 2.

Due to the simplistic network topology in our simulation, the RL-CC RTT and queue-length-based variants are similar. In more complex networks, we conjecture that queue-length will be more robust, though we leave this for future work.

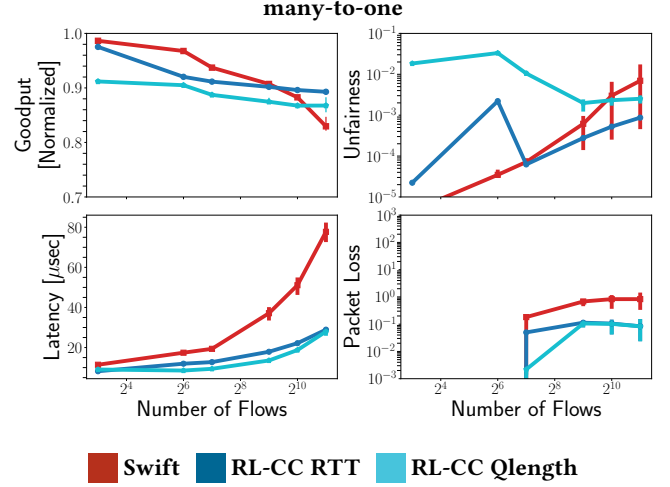


Figure 4: Swift vs. RL-CC RTT vs. RL-CC QLength. Reported results were grouped by total number of flows and obtained with multiple host/flow combinations. Showing group means and 99% confidence intervals. Unfairness is calculated as BW std divided by mean sent BW.

4.1 Explainable RL

One of the biggest concerns of Artificial Intelligence (AI) is that despite its promising success in recent years, it is hard to decipher its decisions in a human interpretable form. Evidently, the literature on explainable AI is growing rapidly [8]. In this section, we analyze the behavior of our RL policy and show how it matches known concepts in classic CC theory.

To support a straightforward input-output relation and allow visualization, we simplified our RL-CC architecture of a multi-layer perceptron (MLP) [34] and used a window of two states, past and present, as input. We inspect three scenarios of interest by setting three representative previous states s_{t-1} : (a) previously in steady-state, (b) previously under-utilized network, and (c) previously congested network. Recall that each state is a 2-dimensional vector, $s_t = (a_{t-1}, \delta_t)$. After fixing s_{t-1} , we then manually scan the two-dimensional input space of s_t and color the corresponding output a_t in Fig. 5. In addition, the arrows point to locations where $s_t = s_{t-1}$.

In Fig. 5 (a), We first see the δ_t has the highest impact on a_t . Then we observe that for the same δ_t the a_{t-1} slightly impact the a_t for $a_{t-1} = 0.85$ or 1.15 we get $a_{t-1} = 1.05$ and 0.95 respectively. This demonstrates how during periods of no change, the policy is to fluctuate gently around the stead state which helps desynchronizing flows and avoiding stronger fluctuations. Next, Fig. 5 (b) and Fig. 5 (c) show symmetric

mirrored behaviors. In both cases, the policy counters overshoots after rate increments/decrements while the impact of a_{t-1} is minimal. We observe that RL-CC is a pro-active, as opposed to re-active, policy. It anticipates the future state by acting based on what is likely to happen, as opposed to waiting for the event itself. More specifically, when the change in the state is small, the policy outputs a neutral action, $a_t \rightarrow 1$ stabilizing the flow’s transmission rate since it reduces overshoot. However, when the change is large the policy reacts rapidly with on-off control.

5 LIGHTWEIGHT RL-CC

As we have verified in the previous section, and as was shown by Tessler et al. [44], RL-CC exhibits impressive results when compared to SOTA RDMA CC algorithms. However, these results rely on *simulation*.

5.1 Limitations of Neural Networks in NICs

We now explain why RL-CC’s neural network (NN) cannot be deployed on present popular NICs with NVIDIA ConnectX-6Dx as an example. RDMA networks typically have low latency, with RTT of roughly $10\mu\text{sec}$. Since CC acts based on RTT, its decision period needs to be significantly less than that. Based on this logic and on our experiments, we thus have a decision time upper bound of $\sim 2\mu\text{sec}$. This limit also corresponds to our implementation of other SOTA CC algorithms.

NVIDIA’s ConnectX-6Dx introduces a programmable congestion control engine that exposes an SDK for CC implementation. The code runs on in-data-path microprocessors that interact quickly with the NIC’s send/receive pipes. This mechanism has a limited amount of global and per-flow memory. Furthermore, the processor’s instruction set does not support floating-point operations or mathematical libraries for implementing deep-learning activation functions. RL-CC’s architecture is composed of two fully-connected layers (input $\rightarrow 32 \rightarrow 16$) followed by an LSTM layer [19] ($16 \rightarrow 16$) and then an output fully-connected layer ($16 \rightarrow 1$), which sums to over 3000 FLOPs. Therefore, we need to store 2753 parameters (weights and biases) in shared memory and 32 flow-specific parameters (LSTM hidden and cell states) in a per-flow memory.

In an effort to satisfy these restrictions, we employed integer quantization [48] and approximated the non-linear activations using lookup tables. Then, we trained policies with smaller neural-network architectures and tested their decision time on the device. The smallest version which still provided satisfying performance was a single fully-connected layer (input $\rightarrow 12$) followed by an LSTM layer ($12 \rightarrow 12$) and

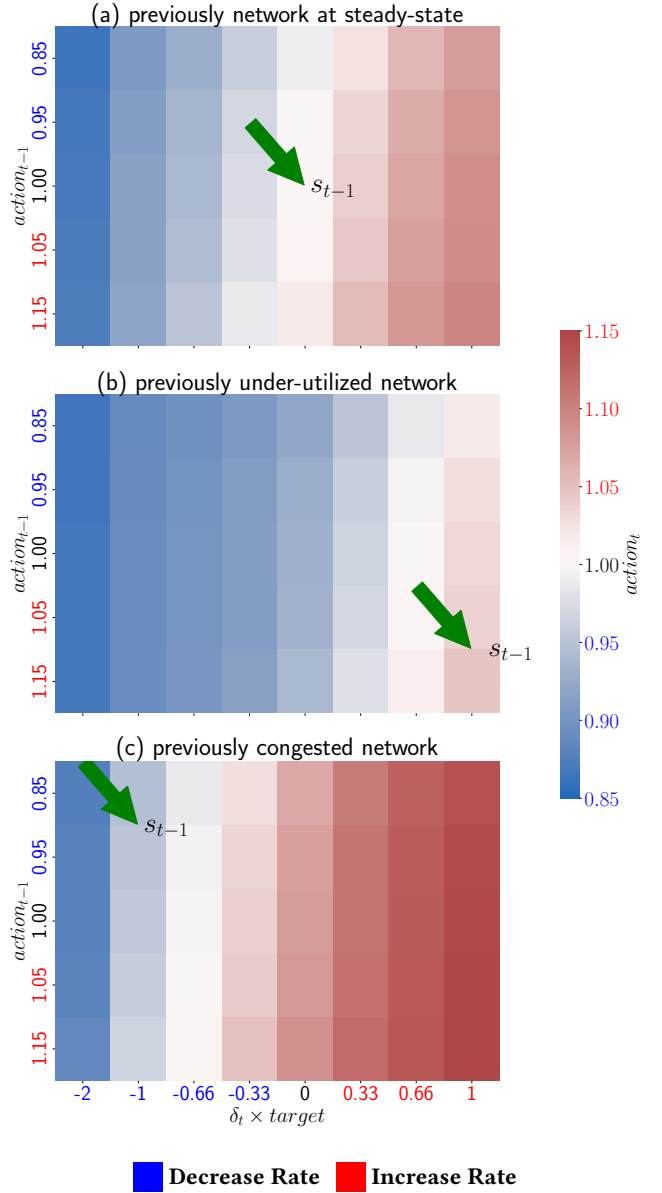


Figure 5: Explaining the RL policy – heatmap of the action output by manually scanning possible state inputs. Green arrows mark the projected position of the previous state s_{t-1} . The leftmost \leftarrow squares denote deep congestion, whereas those to the right \rightarrow denote under-utilization. We analyze three scenarios: (a) network previously in a steady-state; $s_{t-1} = (a_{t-2} = 1, \delta_{t-1} = 0)$, (b) previously a strong increase action due to an under-utilized network; $s_{t-1} = (a_{t-2} = 1.1, \delta_{t-1} = \text{target})$, and (c) previously a strong decrease action was performed due to a congested network; $s_{t-1} = (a_{t-2} = 0.9, \delta_{t-1} = -\text{target})$.

then an output fully connected layer ($12 \rightarrow 1$). The decision latency then varied between $400 - 450\mu\text{sec}$. Next, we dropped

the LSTM layer and instead changed the input to a window of two previous states (input \rightarrow 12 \rightarrow 1), leading to an MLP with a single hidden layer. In this second attempt, the final decision latency was 17 μ sec. Despite this effort, we could not satisfy the desired 2 μ sec limit.

5.2 Boosting-Trees

Boosting-Trees is a suite of machine learning algorithms used for supervised learning tasks such as regression or classification tasks. They often achieve SOTA results on certain tasks and are comparable to deep learning on others [2, 11, 39, 50]. Boosting-Trees are robust [15], deterministic, and once trained, can be easily converted to a sequence of if-else instructions suitable for hardware implementation. We refer specifically to Gradient Boosting Trees (GBT) [35], an ensemble technique that iteratively adds weak tree models (typically CART) to construct a global strong model.

Similar to our RL policy definition, our regression task is to estimate a function $F^* : \mathbb{R}^m \rightarrow \mathbb{R}$ mapping a set of m -dimensional inputs $\mathbf{x} = \{x_1, \dots, x_n\}$ to 1-dimensional outputs $\{y_1, \dots, y_n\}$. This is done by minimizing an expected loss function $L(y, F(x))$ over the training dataset such that

$$\hat{F} = \arg \min_F \mathbb{E}[L(y, F(x))].$$

More specifically, \hat{F} is constructed iteratively as a sequence of estimators such that at each iteration t , $F^t = F^{t-1} + \alpha h^t$, where α is the step-size and $h^t : \mathbb{R}^m \rightarrow \mathbb{R}$ is called the base-predictor. Moreover, h^t is chosen such that

$$h^t = \arg \min_{h \in H} \mathbb{E}[L(y, F^{t-1}(x) + h(x))].$$

In this work, we use CatBoost [37], a SOTA GBT implementation in which each h^t is a binary decision tree.

5.3 Model Distillation with Boosting Trees

Learning an optimal RL policy requires continuous interaction with an environment. NNs handle this task by gradually updating their parameters via stochastic gradient descent. NN-based policies often require millions or even billions of interactions [3] to reach an optimal policy. These interactions are conducted with sub-optimal policies during the learning stage, and mostly do not reflect optimal behavior. It is only after convergence to an optimal policy that such interactions are suitable to be used in a supervised learning setup. Thus, after training our RL policy with a NN, we can take a representative set of interactions and train a supervised learning model, Boosting Trees in our case. We refer to this process as model distillation.

Formally, a student model g learns the behavior of a teacher model f , such that the knowledge obtained by training f is distilled into g . Our goal is to teach a lightweight RL-CC

tree-based policy that imitates a NN-based policy over a representative distribution of inputs. Previous work has shown that model distillation with trees can work well on various tasks [6, 12, 27, 31, 43]. The biggest challenge in distilling the policy is the LSTM layer, which specializes in incorporating past information. We thus removed the LSTM layer and instead provide as input a window of previous states. The distillation process is illustrated in Fig. 6. Its goal is to minimize the loss between the outputs of the two models on data gathered during the NN RL policy inference stage. We restricted the number of boosting iterations and maximal tree depth per tree to satisfy the limits of ConnectX-6Dx. The resulting number of operations does not exceed 150.

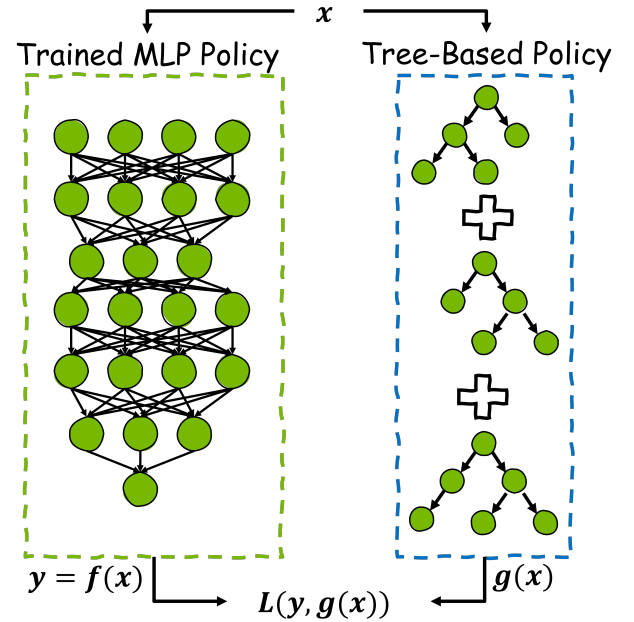


Figure 6: Model Distillation: Teaching tree-based student policy g to mimic the fixed NN-based policy f by minimizing

$$L(y, g(x)) = \sqrt{\frac{1}{N} \sum_{n=1}^N (y_i - g(x_i))^2}.$$

In Table 1, we compare the decision time latency between the original NN and distilled tree-based policies. As seen, we obtained x500 speed-up, from 450 μ sec down to 0.9 μ sec.

In Table 2, we compare the performance differences between the MLP-based teacher model and our tree-based distilled student model. Our results show that using the distillation method, the student is capable of perfectly imitating the performance of the more complex teacher model.

6 EVALUATION

By distilling the NN RL policy to an efficient decision tree, we now satisfy the decision-time constraint of 2 μ sec. We use the programmable CC interface of ConnectX-6Dx and deploy our

	Small LSTM	MLP	Boosting-Trees
FLOPS	2600	200	-
Decision Latency [μsec]	450	17	0.9

Table 1: FLOPS and inference latency as calculated on ConnectX-6Dx. a) Small LSTM: state \rightarrow fc \rightarrow LSTM \rightarrow fc \rightarrow action. b) MLP: window of states \rightarrow fc \rightarrow action. c) Boosting-Trees: implemented as an if-else sequence.

Number of Flows	8		64		512		1024		2048	
Metric	GP	Latency	GP	Latency	GP	Latency	GP	Latency	GP	Latency
RL-CC RTT (MLP)	0.96	8.85	0.92	12.19	0.90	17.82	0.90	21.70	0.90	27.62
RL-CC RTT (Tree)	0.97	8.85	0.92	12.03	0.90	17.98	0.90	21.73	0.90	27.35

Table 2: Policy Distillation: Comparing MLP based policy vs distilled policy on many-to-one scenarios while varying the number of flows. GP denotes Goodput [normalized], and Latency is measured in μsec .

tree-based policy on two live clusters. We begin by describing the cluster setup, and then provide the experimental results.

6.1 Setup

Our setup involves ConnectX-6Dx NICs connected through a Spectrum-2 switch over a lossy network with a link rate of 100 Gbps. We experimented on two operational clusters, detailed below. As both clusters do not support in-network telemetry, the tests were performed with the lightweight RL-CC RTT-based version.

Small cluster - single-rack-traffic tests on a single switch cluster with seven hosts.

Large cluster - inter-rack-traffic tests on a cluster consisting of a two-level Fat-Tree [1] topology with three spines connected via four 100 Gbps links to four Top of the racks (ToRs) each with 16 nodes.

The traffic was generated by continuously posting of 64KB RDMA Write requests to the receiver.

We compared Lightweight RL-CC to DCQCN and Swift. RL-CC was trained on a single-switch OmNeT++ simulation on various many-to-one and all-to-all scenarios, with the parameters set to **target** = 0.064, β = 1.5. We then distilled the trained policy CatBoost [37], with up to 10 boosting trees of a maximal depth of four.

We compared the CC algorithms' ability to maintain a steady state and react to network changes. In the small cluster we performed many-to-one, all-to-all, and long-short tests. In the large cluster we performed many-to-one and all-to-all tests. We tested various configurations of number of flows per host and averaged across them.

6.2 Small Cluster

Beginning with steady-state scenarios, we compare RL-CC with DCQCN and Swift in Fig. 7. In all cases, RL-CC sustains a high goodput bandwidth and low unfairness, similar to

DCQCN and Swift. At the same time, RL-CC achieves substantially lower packet latency and packet loss throughout the many-to-one test. In the all-to-all-test, RL-CC demonstrates minimal packet latency up to 128 flows, after which it exhibits similar behavior to Swift. Although in the large flow regime DCQCN presents better performance, compared to Swift and RL-CC, it is the only method to exhibit packet loss in the mid-range.

Next, we evaluated RL-CC's ability to react to network changes. Fig. 8 compares DCQCN, Swift, and RL-CC in the long-short test. The results show that RL-CC maintains the highest long bandwidth and competitive completion time throughout all the tests, outperforming Swift on both metrics. Additionally, while both Swift and RL-CC did not lose packets, DCQCN incurred packet loss in 100 flows. Moreover, DCQCN displays poor recovery performance with low long bandwidths in all scenarios. These results illustrate RL-CC's ability to rapidly adjust the transmission rate to changes in the network.

Summarizing the small cluster results, RL-CC sustains high bandwidth while reducing packet latency and packet loss. Moreover, tree-based RL-CC displays similar performance on ConnectX-6Dx as on the simulator.

6.3 Large Cluster

Here, we evaluate RL-CC at scale by running steady-state tests on a large cluster with 64 hosts. As RL-CC was trained on a single switch simulator, this environment evaluates its ability to generalize to new and unseen scenarios.

As seen in Fig. 9, RL-CC demonstrates competitive goodput bandwidth compared to Swift in both tests. RL-CC's packet latency is lower than DCQCN and an order of magnitude lower than Swift in the many-to-one test. In the all-to-all test, RL-CC displays slightly lower packet latency than Swift. While RL-CC displays the highest unfairness, its highest value, $\sim 10^{-2}$, is absolutely low. When considering packet

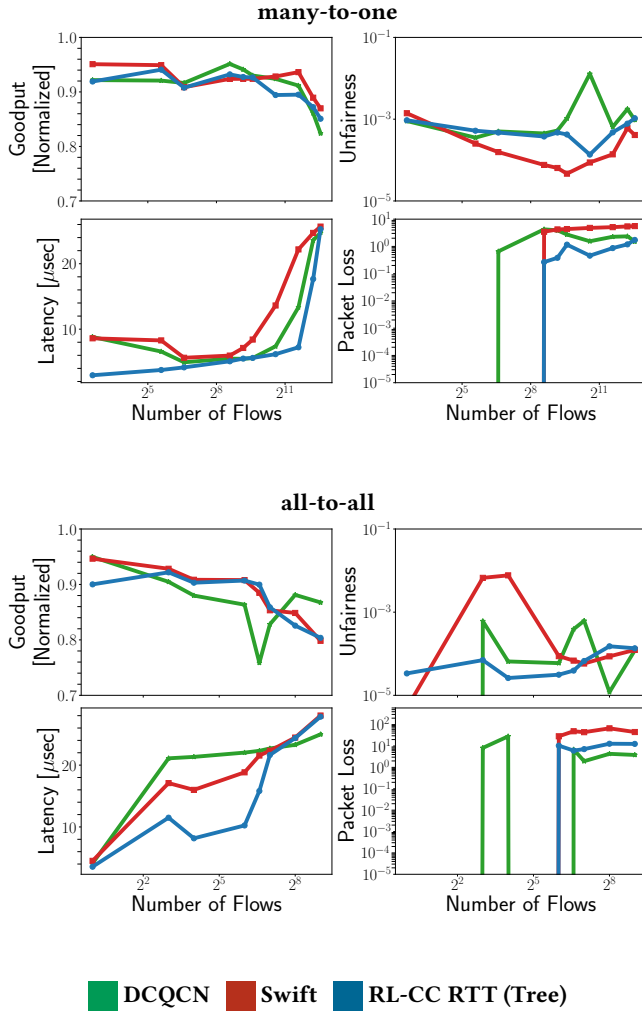


Figure 7: Small seven-host cluster tests. Test duration is 30 sec for all scenarios. Unfairness is calculated as std of BW divided by mean sent BW. Packet loss is the total number of dropped packets divided by number of flows.

loss, RL-CC attained the lowest values throughout all scenarios, while DCQCN is the worst in both tests and exhibited large packet latencies even for a small number of flows. To conclude, RL-CC performed comparably well in the large cluster, demonstrating its ability to perform well at scale.

We conclude our experiments by presenting the behavior over time in Figs. 10 and 11. We focus on the two scenarios with the largest number of flows, one from many-to-one and the other all-to-all. In both figures, the metrics were sampled once per second. This gives a coarse representation of the behavior of each algorithm. DCQCN, Swift, and RL-CC all sustain a stable steady-state goodput bandwidth and a fair sent-bandwidth. These results further validate those

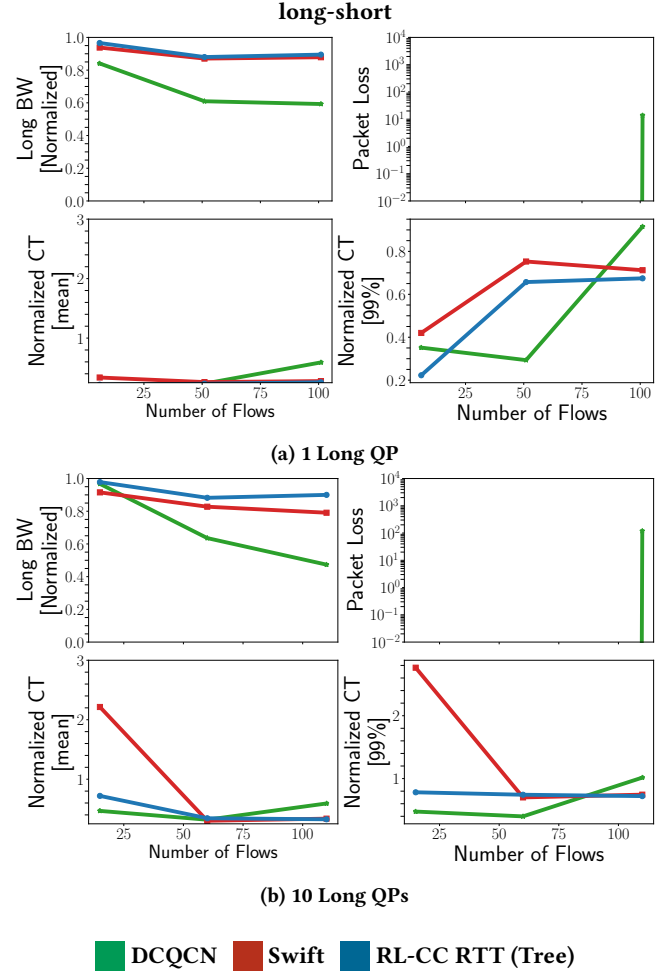


Figure 8: Small seven-host cluster. Long flow duration is 30 sec. Each short flow sends 4MB per node every iteration. Iterations are spaced out with 10ms time difference for a total of 500 iterations. Packet loss is the total number of dropped packets divided by number of flows.

of Fig. 9, indicating that all algorithms exhibit fairness. Interestingly, while all methods incur packet loss during the bring-up phase, RLCC is the only one without continued packet loss in the all-to-all test.

Lastly, Fig. 12 depicts the tradeoff between goodput bandwidth and packet latency / packet loss. RL-CC presents the best overall tradeoff. In many-to-one, RL-CC achieves significantly lower latency and minimal packet loss at the expense of slightly lowering its goodput bandwidth. In all-to-all, RL-CC sustains high bandwidths while keeping similar packet latencies as DCQCN and Swift, with minimal packet loss.

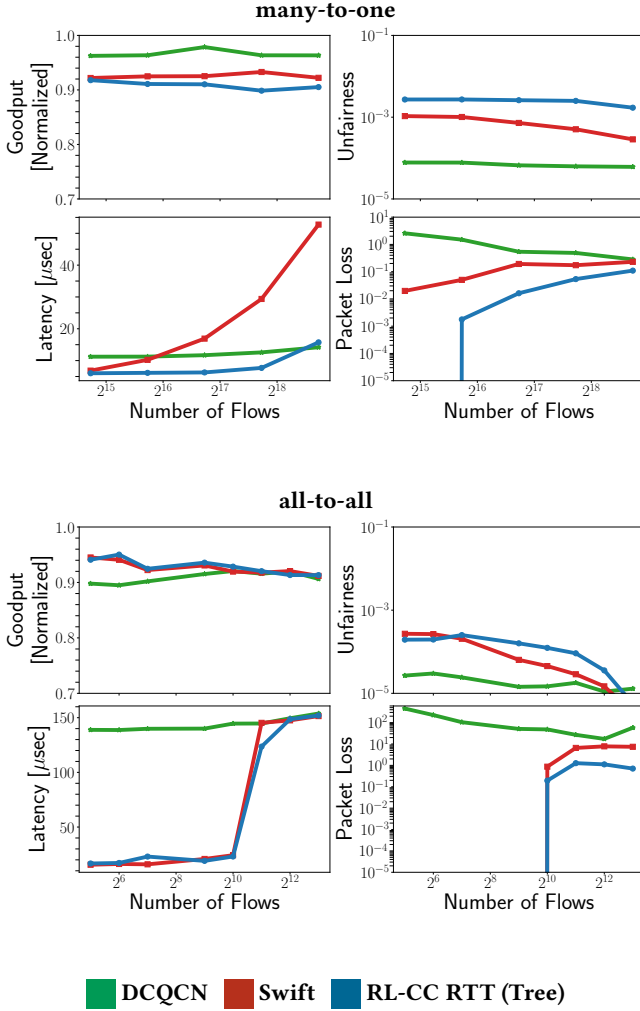


Figure 9: Large 64-host cluster tests. Test duration is 60 sec for both test. Unfairness is calculated as std of BW divided by mean sent BW. Packet loss is the total number of dropped packets divided by number of flows.

7 RELATED WORK

Learning-based approaches have been proposed for efficient CC in various networking applications.

TCP applications. Dong et al. [14] proposed PCC vivace as an online-learning CC algorithm. In PCC Vivace, information is collected during monitor intervals followed by an online learning step optimizing a utility function. PCC Vivace employs methods such as gradient ascent and linear regression, which are challenging to implement directly in a NIC and cannot meet the low decision needs of RDMA. Jay et al. [21] introduced Aurora, a congestion control framework based on deep RL. Similar to PCC vivace, Aurora utilizes information gathered through monitor intervals to define a

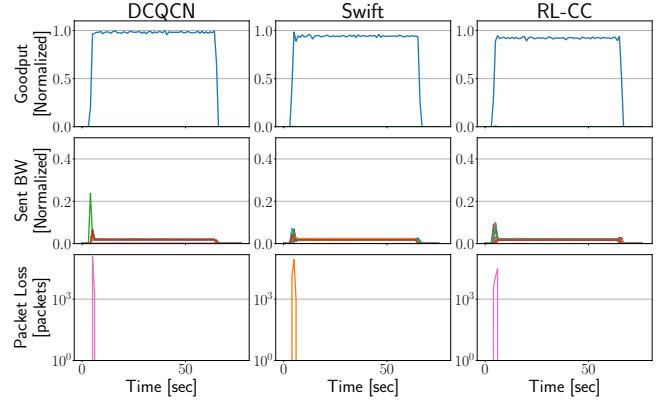


Figure 10: Large 64 host cluster – many-to-one test with 434176 flows. Data was sampled every 1 sec. Different colors denote different hosts.

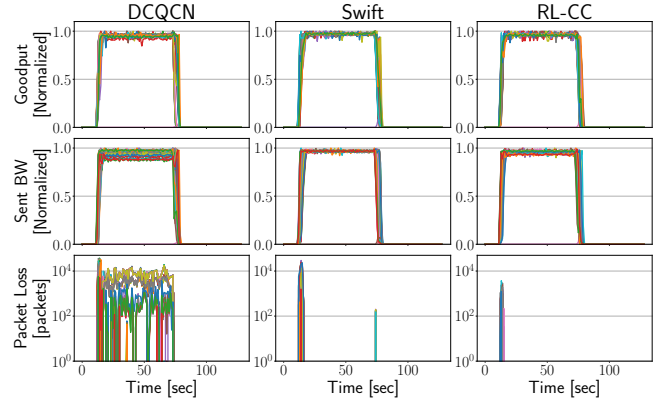


Figure 11: Large 64-host cluster – all-to-all test with 8192 flows. Data was sampled every 1 sec. Different colors denote different hosts.

state, which is then used to optimize a policy via the PPO algorithm [41]. Nonetheless, Tessler et al. [44] reported that Aurora has failed to work when considering a realistic setting. Nie et al. [36] introduced TCP-RL, a deep RL CC algorithm for TCP that dynamically defines the CC configurations and initial window based on network conditions.

Non-TCP networking applications. Jin et al. [24] have proposed two RL-based CC algorithms for software-defined-network datacenters, SDN DCN, off-policy based on Q-learning [46], and an on-policy method based on SARSA [40]. Lan et al. [26] developed DRL-CCP, a deep RL CC algorithm for named data networking. Mai et al. [32] have applied DDPG [30], an RL algorithm, for learning CC strategies in multipath TCP used in satellite networks. Carlucci et al. [10] designed a Kalman Filtering [28] based CC algorithm implemented in the RTP/RTCP protocol [5]. Jiang et al. [23] introduced

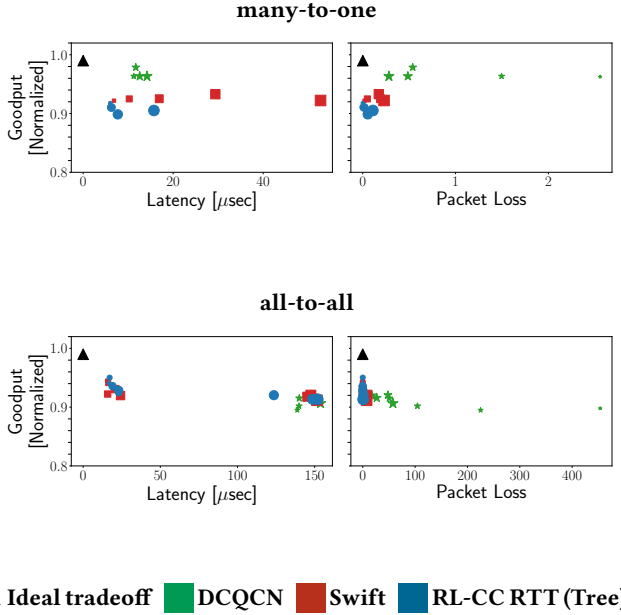


Figure 12: Large 64-host cluster. (Left) goodput vs. latency. (Right) goodput vs. packet loss. Marker size is proportional to the number of flows in the scenario. Packet loss is the total number of dropped packets divided by number of flows.

TCP-G Vegas that employs Q-learning to increase throughput in multi-hop ad hoc networks.

Learning-based methods in general and RL in particular have many applications in networking. Nevertheless, the computational and memory requirements of NN training and inference are too demanding for implementation on NICs such as ConnectX-6Dx. Wei et al. [47] proposed a lightweight CC framework with deep RL to prune policies by 50%. Albeit, the result is still too demanding for ConnectX-6Dx. To the best of our knowledge, our RL-CC implementation is the first learning-based RDMA CC algorithm applied outside of simulation.

8 CONCLUSION AND FUTURE DIRECTIONS

Effective CC is crucial for high network performance in modern datacenters. The benefit of machine learning methods is their ability to extract meaningful patterns from complex data, often making them better than humans in such tasks. To the best of our knowledge, we presented here for the first time in literature a machine learning CC method that can successfully run in real-time within operational datacenters.

On the path to deployment, we began with an extensive analysis of RL-CC. We performed a thorough study of the various tradeoffs in reward design, and showed RL-CC's

ability to track the theoretical inflation curves. We then examined how and why the learned policy makes decisions. We inspected output sensitivity to combinations of prior and present states. This analysis sheds a light on the feasibility of a data-driven MIMD approach, challenging prior belief that AIMD is required to converge to a stable and fair solution.

When considering real-time deployment in hardware, the agent, initially represented using a NN, required $450\mu\text{sec}$ to perform inference. Due to the rate of change within the datacenter, this resulted in an inability to control congestion. We introduced a method for distilling the agent to decision trees, reducing the inference time down to $0.9\mu\text{sec}$, a x500 improvement.

Finally, we deployed RL-CC on a real cluster, consisting of 64 hosts, running in real time on ConnectX-6Dx NICs. RL-CC demonstrated high goodput and fairness while retaining low packet latency and minimal packet loss. Moreover, we showed the ability of RL-CC to generalize, out of the box, to new and unseen scenarios.

Our tree-based RL-CC is an initial step towards real-world lightweight AI CC. AI methods generally perform better when trained on larger and richer data. In future work, we aim to study additional network signals that may enable better prediction of the network state. An additional potential candidate to benefit from AI algorithms is the switch. There, not only congestion control is possible, but also power optimization, efficient routing, and more.

REFERENCES

- [1] Mohammad Al-Fares, Alexander Loukissas, and Amin Vahdat. 2008. A Scalable, Commodity Data Center Network Architecture. In *Proceedings of the ACM SIGCOMM 2008 Conference on Data Communication (Seattle, WA, USA) (SIGCOMM '08)*. Association for Computing Machinery, New York, NY, USA, 63–74. <https://doi.org/10.1145/1402958.1402967>
- [2] Ionut Anghel, Tudor Cioara, Dorin Moldovan, Ioan Salomie, and Madalina Maria Tomus. 2018. Prediction of Manufacturing Processes Errors: Gradient Boosted Trees Versus Deep Neural Networks. In *2018 IEEE 16th International Conference on Embedded and Ubiquitous Computing (EUC)*. 29–36. <https://doi.org/10.1109/EUC.2018.00012>
- [3] Adrià Puigdomènech Badia, Bilal Piot, Steven Kapturowski, Pablo Sprechmann, Alex Vitvitskiy, Zhaohan Daniel Guo, and Charles Blundell. 2020. Agent57: Outperforming the atari human benchmark. In *International Conference on Machine Learning*. PMLR, 507–517.
- [4] Motti Beck and Michael Kagan. 2011. Performance evaluation of the RDMA over ethernet (RoCE) standard in enterprise data centers infrastructure. In *Proceedings of the 3rd Workshop on Data Center Converged and Virtual Ethernet Switching*. 9–15.
- [5] Adam Bergkvist, Daniel C Burnett, Cullen Jennings, Anant Narayanan, and Bernard Aboba. 2012. WebRTC 1.0: Real-time communication between browsers. *Working draft, W3C 91* (2012), 2012.
- [6] Max Biggs, Wei Sun, and Markus Etzl. 2020. Model Distillation for Revenue Optimization: Interpretable Personalized Pricing.
- [7] Van-Phuc Bui, Trinh Van Chien, Eva Lagunas, Joël Grotz, Symeon Chatzinotas, and Björn Ottersten. 2021. Robust Congestion Control for

- Demand-Based Optimization in Precoded Multi-Beam High Throughput Satellite Communications. <https://doi.org/10.48550/ARXIV.2109.02327>
- [8] Nadia Burkart and Marco F. Huber. 2021. A Survey on the Explainability of Supervised Machine Learning. *Journal of Artificial Intelligence Research* 70 (jan 2021), 245–317. <https://doi.org/10.1613/jair.1.12228>
 - [9] Idan Burstein. 2021. Nvidia Data Center Processing Unit (DPU) Architecture. In *2021 IEEE Hot Chips 33 Symposium (HCS)*. IEEE, 1–20.
 - [10] Gaetano Carlucci, Luca De Cicco, Stefan Holmer, and Saverio Mascolo. 2016. Analysis and Design of the Google Congestion Control for Web Real-Time Communication (WebRTC). In *Proceedings of the 7th International Conference on Multimedia Systems (Klagenfurt, Austria) (MMSys '16)*. Association for Computing Machinery, New York, NY, USA, Article 13, 12 pages. <https://doi.org/10.1145/2910017.2910605>
 - [11] Rich Caruana and Alexandru Niculescu-Mizil. 2006. An Empirical Comparison of Supervised Learning Algorithms. In *Proceedings of the 23rd International Conference on Machine Learning (Pittsburgh, Pennsylvania, USA) (ICML '06)*. Association for Computing Machinery, New York, NY, USA, 161–168. <https://doi.org/10.1145/1143844.1143865>
 - [12] Zhengping Che, Sanjay Purushotham, Robinder Khemani, and Yan Liu. 2017. Interpretable Deep Models for ICU Outcome Prediction. *AMIA ... Annual Symposium proceedings. AMIA Symposium* 2016 (10 Feb 2017), 371–380. [https://pubmed.ncbi.nlm.nih.gov/28269832/28269832\[pmid\]](https://pubmed.ncbi.nlm.nih.gov/28269832/28269832[pmid]).
 - [13] Dah-Ming Chiu and Raj Jain. 1989. Analysis of the increase and decrease algorithms for congestion avoidance in computer networks. *Computer Networks and ISDN Systems* 17, 1 (1989), 1–14. [https://doi.org/10.1016/0169-7552\(89\)90019-6](https://doi.org/10.1016/0169-7552(89)90019-6)
 - [14] Mo Dong, Tong Meng, Doron Zarchy, Engin Arslan, Yossi Gilad, Brighten Godfrey, and Michael Schapira. 2018. PCC Vivace: Online-Learning Congestion Control. In *15th USENIX Symposium on Networked Systems Design and Implementation (NSDI 18)*. USENIX Association, Renton, WA, 343–356. <https://www.usenix.org/conference/nsdi18/presentation/dong>
 - [15] Gil Einziger, Maayan Goldstein, Yaniv Sa'ar, and Itai Segall. 2019. Verifying Robustness of Gradient Boosted Models. In *Proceedings of the Thirty-Third AAAI Conference on Artificial Intelligence and Thirty-First Innovative Applications of Artificial Intelligence Conference and Ninth AAAI Symposium on Educational Advances in Artificial Intelligence (Honolulu, Hawaii, USA) (AAAI'19/IAAI'19/EAAI'19)*. AAAI Press, Article 302, 8 pages. <https://doi.org/10.1609/aaai.v33i01.33012446>
 - [16] S. Floyd. 2003. RFC3649: HighSpeed TCP for Large Congestion Windows.
 - [17] Sally Floyd, Dr. K. K. Ramakrishnan, and David L. Black. 2001. The Addition of Explicit Congestion Notification (ECN) to IP. RFC 3168. <https://doi.org/10.17487/RFC3168>
 - [18] Chuanxiong Guo, Haitao Wu, Zhong Deng, Gaurav Soni, Jianxi Ye, Jitu Padhye, and Marina Lipshteyn. 2016. RDMA over Commodity Ethernet at Scale. In *Proceedings of the 2016 ACM SIGCOMM Conference (Florianopolis, Brazil) (SIGCOMM '16)*. Association for Computing Machinery, New York, NY, USA, 202–215. <https://doi.org/10.1145/2934872.2934908>
 - [19] Sepp Hochreiter and Jürgen Schmidhuber. 1997. Long Short-Term Memory. *Neural Comput.* 9, 8 (nov 1997), 1735–1780. <https://doi.org/10.1162/neco.1997.9.8.1735>
 - [20] Shuihai Hu, Yibo Zhu, Peng Cheng, Chuanxiong Guo, Kun Tan, Jitendra Padhye, and Kai Chen. 2016. Deadlocks in Datacenter Networks: Why Do They Form, and How to Avoid Them. In *Proceedings of the 15th ACM Workshop on Hot Topics in Networks (Atlanta, GA, USA) (HotNets '16)*. Association for Computing Machinery, New York, NY, USA, 92–98. <https://doi.org/10.1145/3005745.3005760>
 - [21] Nathan Jay, Noga Rotman, Brighten Godfrey, Michael Schapira, and Aviv Tamar. 2019. A Deep Reinforcement Learning Perspective on Internet Congestion Control. In *Proceedings of the 36th International Conference on Machine Learning (Proceedings of Machine Learning Research, Vol. 97)*, Kamalika Chaudhuri and Ruslan Salakhutdinov (Eds.). PMLR, 3050–3059. <https://proceedings.mlr.press/v97/jay19a.html>
 - [22] Huiling Jiang, Qing Li, Yong Jiang, Gengbiao Shen, Richard O. Sinnott, Chen Tian, and Mingwei Xu. 2020. When Machine Learning Meets Congestion Control: A Survey and Comparison. *CoRR* abs/2010.11397 (2020). arXiv:2010.11397 <https://arxiv.org/abs/2010.11397>
 - [23] Hong Jiang, Ying Luo, Qiuyun Zhang, Mingyong Yin, and Chun Wu. 2017. TCP-Gvegas with Prediction and Adaptation in Multi-Hop Ad Hoc Networks. *Wirel. Netw.* 23, 5 (jul 2017), 1535–1548. <https://doi.org/10.1007/s11276-016-1242-y>
 - [24] Rong Jin, Jiaojiao Li, Xin Tuo, Weiming Wang, and Xiaolin Li. 2018. A congestion control method of SDN data center based on reinforcement learning. *International Journal of Communication Systems* 31, 17 (2018), e3802. <https://doi.org/10.1002/dac.3802> arXiv:https://onlinelibrary.wiley.com/doi/pdf/10.1002/dac.3802 e3802 IJCS-18-0005.R1.
 - [25] Gautam Kumar, Nandita Dukkkipati, Keon Jang, Hassan M. G. Wassel, Xian Wu, Behnam Montazeri, Yaogong Wang, Kevin Springborn, Christopher Alfeld, Michael Ryan, David Wetherall, and Amin Vahdat. 2020. Swift: Delay is Simple and Effective for Congestion Control in the Datacenter. In *Proceedings of the Annual Conference of the ACM Special Interest Group on Data Communication on the Applications, Technologies, Architectures, and Protocols for Computer Communication (Virtual Event, USA) (SIGCOMM '20)*. Association for Computing Machinery, New York, NY, USA, 514–528. <https://doi.org/10.1145/3387514.3406591>
 - [26] Dehao Lan, Xiaobin Tan, Jinyang Lv, Yang Jin, and Jian Yang. 2019. A Deep Reinforcement Learning Based Congestion Control Mechanism for NDN. In *ICC 2019 - 2019 IEEE International Conference on Communications (ICC)*. 1–7. <https://doi.org/10.1109/ICC.2019.8761737>
 - [27] Jiawei Li, Yiming Li, Xingchun Xiang, Shu-Tao Xia, Siyi Dong, and Yun Cai. 2020. TNT: An Interpretable Tree-Network-Tree Learning Framework using Knowledge Distillation. *Entropy* 22, 11 (2020). <https://doi.org/10.3390/e22111203>
 - [28] Qiang Li, Ranyang Li, Kaifan Ji, and Wei Dai. 2015. Kalman Filter and Its Application. In *2015 8th International Conference on Intelligent Networks and Intelligent Systems (ICINIS)*. 74–77. <https://doi.org/10.1109/ICINIS.2015.35>
 - [29] Yuliang Li, Rui Miao, Hongqiang Harry Liu, Yan Zhuang, Fei Feng, Lingbo Tang, Zheng Cao, Ming Zhang, Frank Kelly, Mohammad Alizadeh, and Minlan Yu. 2019. HPCC: High Precision Congestion Control. In *Proceedings of the ACM Special Interest Group on Data Communication (Beijing, China) (SIGCOMM '19)*. Association for Computing Machinery, New York, NY, USA, 44–58. <https://doi.org/10.1145/3341302.3342085>
 - [30] Timothy P. Lillicrap, Jonathan J. Hunt, Alexander Pritzel, Nicolas Heess, Tom Erez, Yuval Tassa, David Silver, and Daan Wierstra. 2015. Continuous control with deep reinforcement learning. <https://doi.org/10.48550/ARXIV.1509.02971>
 - [31] Xuan Liu and Xiaoguang Wang. 2018. Improving the Interpretability of Deep Neural Networks with Knowledge Distillation. 905–912. <https://doi.org/10.1109/ICDMW.2018.00132>
 - [32] Tianle Mai, Haipeng Yao, Yaqing Jing, Xiaobin Xu, Xiaolong Wang, and Zhe Ji. 2019. Self-learning Congestion Control of MPTCP in Satellites Communications. In *2019 15th International Wireless Communications & Mobile Computing Conference (IWCMC)*. 775–780. <https://doi.org/10.1109/IWCMC.2019.8766465>
 - [33] Radhika Mittal, Vinh The Lam, Nandita Dukkkipati, Emily Blem, Hassan Wassel, Monia Ghobadi, Amin Vahdat, Yaogong Wang, David Wetherall, and David Zats. 2015. TIMELY: RTT-Based Congestion Control

- for the Datacenter. *SIGCOMM Comput. Commun. Rev.* 45, 4 (aug 2015), 537–550. <https://doi.org/10.1145/2829988.2787510>
- [34] Fionn Murtagh. 1991. Multilayer perceptrons for classification and regression. *Neurocomputing* 2, 5 (1991), 183–197. [https://doi.org/10.1016/0925-2312\(91\)90023-5](https://doi.org/10.1016/0925-2312(91)90023-5)
- [35] Alexey Natekin and Alois Knoll. 2013. Gradient boosting machines, a tutorial. *Frontiers in neurorobotics* 7 (2013), 21.
- [36] Xiaohui Nie, Youjian Zhao, Zhihan Li, Guo Chen, Kaixin Sui, Jiyang Zhang, Zijie Ye, and Dan Pei. 2019. Dynamic TCP Initial Windows and Congestion Control Schemes Through Reinforcement Learning. *IEEE Journal on Selected Areas in Communications* PP (03 2019), 1–1. <https://doi.org/10.1109/JSAC.2019.2904350>
- [37] Liudmila Prokhorenkova, Gleb Gusev, Aleksandr Vorobev, Anna Veronika Dorogush, and Andrey Gulin. 2018. CatBoost: unbiased boosting with categorical features. In *Advances in Neural Information Processing Systems*, S. Bengio, H. Wallach, H. Larochelle, K. Grauman, N. Cesa-Bianchi, and R. Garnett (Eds.), Vol. 31. Curran Associates, Inc. <https://proceedings.neurips.cc/paper/2018/file/14491b756b3a51daac41c24863285549-Paper.pdf>
- [38] Martin L. Puterman. 1994. *Markov decision processes: discrete stochastic dynamic programming*. John Wiley and Sons.
- [39] Byron P. Roe, Hai-Jun Yang, Ji Zhu, Yong Liu, Ion Stancu, and Gordon McGregor. 2005. Boosted decision trees as an alternative to artificial neural networks for particle identification. *Nuclear Instruments and Methods in Physics Research Section A: Accelerators, Spectrometers, Detectors and Associated Equipment* 543, 2–3 (May 2005), 577–584. <https://doi.org/10.1016/j.nima.2004.12.018>
- [40] G. Rummery and Mahesan Niranjan. 1994. On-Line Q-Learning Using Connectionist Systems. *Technical Report CUED/F-INFENG/TR 166* (11 1994).
- [41] John Schulman, Filip Wolski, Prafulla Dhariwal, Alec Radford, and Oleg Klimov. 2017. Proximal Policy Optimization Algorithms. <https://doi.org/10.48550/ARXIV.1707.06347>
- [42] Alexander Shpiner, Eitan Zahavi, Omar Dahley, Aviv Barnea, Rotem Damsker, Gennady Yekelis, Michael Zus, Eitan Kuta, and Dean Baram. 2017. RoCE Rocks without PFC: Detailed Evaluation. In *Proceedings of the Workshop on Kernel-Bypass Networks* (Los Angeles, CA, USA) (*KBNet '17*). Association for Computing Machinery, New York, NY, USA, 25–30. <https://doi.org/10.1145/3098583.3098588>
- [43] Jie Song, Haofei Zhang, Xinchao Wang, Mengqi Xue, Ying Chen, Li Sun, Dacheng Tao, and Mingli Song. 2021. Tree-Like Decision Distillation. In *Proceedings of the IEEE/CVF Conference on Computer Vision and Pattern Recognition (CVPR)*. 13488–13497.
- [44] Chen Tessler, Yuval Shpigelman, Gal Dalal, Amit Mandelbaum, Doron Haritan Kazakov, Benjamin Führer, Gal Chechik, and Shie Mannor. 2022. Reinforcement learning for datacenter congestion control. *ACM SIGMETRICS Performance Evaluation Review* 49, 2 (2022), 43–46.
- [45] András Varga. 2002. OMNeT++ <http://www.omnetpp.org>. *IEEE Network Interactive* 16, 4 (2002).
- [46] Christopher J.C.H. Watkins and Peter Dayan. 1992. Technical Note: Q-Learning. *Machine Learning* 8, 3 (01 May 1992), 279–292. <https://doi.org/10.1023/A:1022676722315>
- [47] Dehui Wei, Jiao Zhang, Xuan Zhang, and Chengyuan Huang. 2022. Plume: Lightweight and generalized congestion control with deep reinforcement learning. *China Communications* (2022), 1–17. <https://doi.org/10.23919/JCC.2022.00.019>
- [48] Hao Wu, Patrick Judd, Xiaojie Zhang, Mikhail Isaev, and Paulius Micikevicius. 2020. Integer Quantization for Deep Learning Inference: Principles and Empirical Evaluation. <https://doi.org/10.48550/ARXIV.2004.09602>
- [49] Guoyuan Yuan, Renjie Zhou, Dezun Dong, and Shan Huang. 2021. Breaking One-RTT Barrier: Ultra-Precise and Efficient Congestion Control in Datacenter Networks. In *2021 International Conference on Computer Communications and Networks (ICCCN)*. 1–9. <https://doi.org/10.1109/ICCCN52240.2021.9522362>
- [50] Chongsheng Zhang, Changchang Liu, Xiangliang Zhang, and George Almpandis. 2017. An Up-to-Date Comparison of State-of-the-Art Classification Algorithms. *Expert Syst. Appl.* 82, C (oct 2017), 128–150. <https://doi.org/10.1016/j.eswa.2017.04.003>
- [51] Yiran Zhang, Yifan Liu, Qingkai Meng, and Fengyuan Ren. 2021. Congestion Detection in Lossless Networks. In *Proceedings of the 2021 ACM SIGCOMM 2021 Conference (Virtual Event, USA) (SIGCOMM '21)*. Association for Computing Machinery, New York, NY, USA, 370–383. <https://doi.org/10.1145/3452296.3472899>
- [52] Renjie Zhou, Dezun Dong, Shan Huang, and Yang Bai. 2021. Fast-Tune: Timely and Precise Congestion Control in Data Center Network. In *2021 IEEE Intl Conf on Parallel and Distributed Processing with Applications, Big Data and Cloud Computing, Sustainable Computing and Communications, Social Computing and Networking (ISPA/BDCLOUD/SocialCom/SustainCom)*. 238–245. <https://doi.org/10.1109/ISPA-BDCLOUD-SocialCom-SustainCom52081.2021.00043>
- [53] Yibo Zhu, Haggai Eran, Daniel Firestone, Chuanxiong Guo, Marina Lipshteyn, Yehonatan Liron, Jitendra Padhye, Shachar Raindel, Mohammad Haj Yahia, and Ming Zhang. 2015. Congestion Control for Large-Scale RDMA Deployments. In *Proceedings of the 2015 ACM Conference on Special Interest Group on Data Communication* (London, United Kingdom) (*SIGCOMM '15*). Association for Computing Machinery, New York, NY, USA, 523–536. <https://doi.org/10.1145/2785956.2787484>